Laser Doppler Measurements of Flow in Freeboard of a Fluidized Bed

One of the factors which reduces combustion efficiency in a fluidized-bed combustor is the elutriation of fine coal particles from the freeboard above the bed surface. To our knowledge, data about the real local flow behavior of the two-phase flow in the freeboard are lacking in the literature. This paper concerns the measurement of the gas and the elutriated particle velocities in the freeboard of a cold fluidized bed using Laser Doppler Anemometry. A special electronic system has been devised to record simultaneously the gas and particle velocities and to indicate the size of the particles. In this paper the apparatus and some preliminary measurements are reported. The most significant observation is that the gas velocity profiles exhibit minima near the bed center and maxima near the walls.

Y. LEVY

Technion—Israel Institute of Technology
Technion City, Haifa, Israel

F. C. LOCKWOOD

Mechanical Engineering Department
Imperial College of Science and Technology
London, England

SCOPE

The potential of fluidized-bed combustors to burn a wide range of fuels in a relatively pollution-free manner has led to a considerable development effort. As yet, there is little commercial exploitation, but there seems little doubt that this will ultimately occur. A development problem of concern is the elutriation or loss of particulate material, including fuel, from the freeboard region. Although this may be cycloned off and returned to the bed, the loss of combustion efficiency due to even quite small amounts of material carried over may become significant compared with the corresponding loss in conventional PF diffusion firing where combustion efficiencies of at least 99% are generally achievable in large boilers such as those used for electricity generation.

The elutriation problem has all the same been somewhat neglected compared with the research effort devoted to the initially more important bubble flow and combustion mechanisms within the bed itself. As a result, the engineer wishing to design prototype fluidized combustor systems is all too often heard to demand of researchers, "but how much how high?" in connection with the elutriation problem. Unfortunately the research performed on this problem has been insufficient to allow a satisfactorily reliable answer.

Brief literature reviews are presented by Lin et al. (1981) and more recently by Kuni and Levenspiel (1977). The existing studies may be broadly classified as: empirically-based works by Leva (1951), Thomas et al. (1961), Lewes et al. (1962), Wen and Hashmgerl (1960), Merrick and Highley (1972); or theoretically-based works by Zenz and Weil (1958), Andrew (1960), Leva and Wen (1971), Chen and Saxena (1978), and Gugnoni and Zenz (1980). We would tentatively summarize the results of these studies as follows. A variety of correlations for the elutriation rate above TDH (transport disengaging height defined as the maximum height attained by those particles whose terminal velocities exceed the local gas mean velocity) are proposed, but none of these appears to offer any degree of universality, order of magnitude discrepancies being typical. None of the studies provides firm information about the particle ejection velocities at the bed surface or about the gas flow field in the freeboard. At best one may conclude that, for the more interesting case of batch operated beds, the concentration of fine particles in the dense bed decays exponentially with time. And that for beds operated in the steady state with freeboard heights lower than the TDH, the elutriation rate of a particle-size group decays exponentially with height above bed.

The existing elutriation measurements have all been performed using mechanical separation devices. Now while this approach may reveal the anomalies of the elutriation phenomenon, it is incapable of revealing their sources. Detailed information about the local gas and particle velocity fields throughout the freeboard region is required. Some particle velocity data have been collected by Do et al. (1972) with the aid of a fast movie camera. Gas velocity measurements have been made using a hot wire technique by Fournol et al. (1973) and Horio et al. (1980); sand particles velocity measurements have been made by the latter using a fiber optic probe. As interesting as these researches are, the very important nature of the particle/gas interaction is not revealed.

The purpose of the present study is to gain new insight into this interaction by employing laser doppler anemometry to perform simultaneous gas and particle velocity measurements in the freeboard region. This task has necessitated the development of the basic laser doppler technique for gas-phase measurement to accommodate the particulate phase as well. The full description of the instrumentation (Levy, 1982) is beyond the scope of this paper. This paper will emphasize the fluid mechanical and combustion interpretation of the data collected.

CONCLUSIONS AND SIGNIFICANCE

The large particulate carryover from the freeboard of fluidized beds is very significantly influenced by the large velocity fluctuations resulting from the bubble eruptions. The turbulence intensities are typically much larger than those of conventional shear-produced turbulence rendering simple calculations based on time-averaged velocities inappropriate. Additionally, the gas velocity profile exhibits a maximum near a wall. This is a previously unknown feature of freeboard flows; it has always been assumed that some sort of duct flow profile, exhibiting a maximum on the centerline, would apply. Greater elutriation rates must be expected near walls.

Since the extent of the region of significantly augmented gas velocities near walls is not small, occupying at least a third of the surface area of the present fairly large experimental bed, it seems likely that the lack of universality of the prevous elutriation measurements is to some extent due to the fact that the majority of the data have been collected on beds of relatively small dimensions. All other operating conditions being equal there is no reason why data collected on one bed in the absence of wall effects should not be duplicated by measurements on another. It should be possible to elucidate universal elutriation laws once we are in a position to superimpose local particle

number counts on the current velocity measurements. The existing LDA is currently being extended to do this.

It is also of interest to apply generalized computer prediction codes developed for conventional pulverized fuel (PF) fired combustors (e.g., Gosman et al., 1978) to the freeboard problem. In principal there is no difficulty in doing this, but two factors complicate the application. First, the magnitude of the velocity fluctuations is so large that the existing turbulence models and particulate/turbulence interaction models may prove inadequate. The degree of inadequacy will, however, probably not be excessive.

The more important difficulty may well prove to be the prescription of initial boundary conditions at the bed surface. The random nature of the bubble eruptions can probably be accommodated by a boundary condition formulated in terms of a (near Gaussian) probability density function, but a suitable boundary description for the vortex rings shed by the eruptions, as well as the specification of an appropriate field finite-difference grid to allow their histories to be satisfactorily computed, represent very challenging problems. If, however, the PF codes can be convincingly applied to the freeboard flow, it is possible to predict and compare the particle carryover, and particle and volatiles combustion, for selected freeboard geometries.

EXPERIMENTAL EQUIPMENT

Fluidized Bed and Traversing Table

The bed cross section had to be great enough to avoid slug flow and other major effects of wall interference. An upper limit was imposed by the necessity to restrict the optical length to a convenient magnitude for the LDA system. After consultation with the United Kingdom National Coal Board, a cross section of 0.3 m by 0.6 m was chosen. The LDA was positioned to traverse the smaller dimensions. The total bed height was 2.4 m. Figure 1 presents a sketch of the fluidized-bed apparatus. It is clear that a bed of this size is far too large to operate with combustion within the confines of a university laboratory and all the experiments were performed for a bed of inert sand particles. Air was supplied through an orifice meter to a plenum chamber whose top surface was a thick porous bronze distribution plate (Accumatic Engineering Sintercon bronze grade "D") giving an even flow distribution. The air then passed through the sand particles (mean diameter = 1.0 mm or 0.4 mm) which form the bed material and escaped via the freeboard region to the surroundings.

The two larger walls (0.6 m × 2.4 m) of the fluidized bed were 19-mm-thick (Pilkington) float glass, clear enough to enable the laser beam to pass with minimal disturbance and strong enough to resist the pressure forces during the operation of the bed. The entire bed structure was bolted to the ground to minimize wall deflections. The walls remained flat and parallel during operation, and the effect of vibration on the optical measurements was insignificant. The consistency of the air flow supply rate was checked and found to vary by less than 1% over a period of 6 hours. Rapid, easy-to-use facilities for filling the bed and draining the sand were incorporated for the general maintenance of and changing of the bed material. Pressure taps were installed at several locations to measure the pressure drops across the distribution plate and the sand, and to record the static pressure within the freeboard.

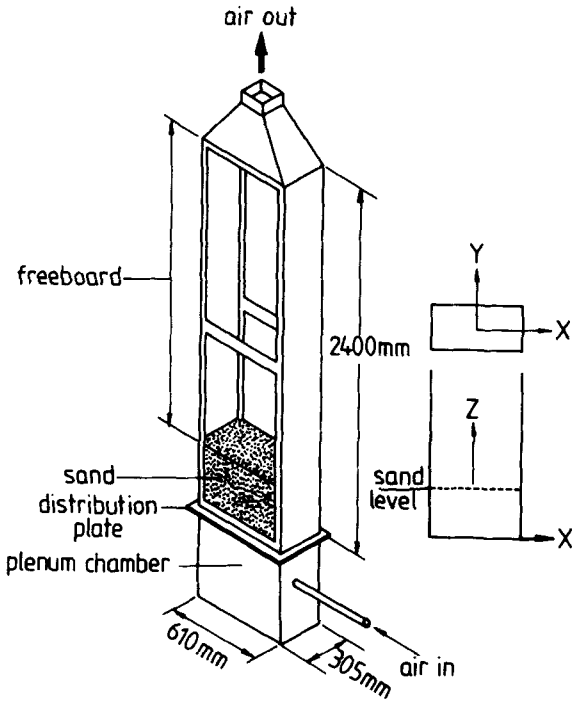

Figure 1. Sketch of the fluidized bed.

Special apparatus was devised to allow controlled single-bubble releases from a nozzle located at the centroid of the distributor plate. Compressed air was fed through a filter and a fine pressure regulator to a settling reservoir. The air then flowed via a solenoid valve to the nozzle. Several nozzle geometries were tested to find one which produced bubbles of consistent and regular shape. A specially built electronic control unit governed the valve cycle and opening times. The volume releases were calibrated as a function of delivery pressure and solenoid opening times. For a fixed setting of these variables the variation of volumes from successive openings was less than 5%.

It was desirable to traverse the whole of the freeboard. The use of a vertical drilling machine ("Pollard" Model 150), with an additional column to double its vertical travel, enabled this to be done effectively and cheaply. A 600 mm × 600 mm X-Y traversing table (Unimatic Engineers Ltd. type 600) was secured to the top of the vertical table so permitting continuous traversing of 600 mm × 600 mm × 1,200 mm.

Optical System

A standard forward scatter Laser Doppler Anemometer optical system with frequency shift formed the basis of the instrumentation. The components of the system were: a 5 mw HeNe laser (Spectra Physics model 120), a beam splitter, and Bragg cell (DISA 55X modular LDA optics), and a photomultiplier (E.M.I. 9817b). The components in the photomultiplier unit were chosen to provide as linear a response as possible over the whole of the light intensity range. The important optical dimensions were: beam spacing = 60 mm; half beam crossing angle = 3.9°; magnification of the collecting optics = 3.0; pinhole diameter = 0.50 mm.

Two-Phase Flow Measurements and Signal Processing

Real bed material consists mainly of sand (and sometimes limestone) particles of about 1,000-μm diameter plus typically 1% of fuel. In the present simulation one would ideally want to determine sand and gas velocities and the sand particle diameters as well. No suitable and developed technique could be uncovered in the literature. The inclusion of particle diameter measurement considerably complicates the problem, and the decision was made to eliminate it from the list by making measurements in beds of (nearly) monosize sand particles, the size being varied across the range of practical interest in a series of experiments. The relatively small influence of the fuel is ignored.

The selected, and to our minds the most convenient, principle of discrimination between the two-phase velocity measurements is based on the fact that there is a direct relation between particle size and the intensity of the scattered light (i.e., signal amplitude). A schematic drawing of a typical signal detected by the photomultiplier is given in Figure 2(a). The relation between signal amplitude and particle size has been investigated Ugut et al. (1978), and Durst and Elisson (1976), but neither of these concerned the present case of solid particles much bigger than the control volume diameter. For the present particles initial tests indicated a clear

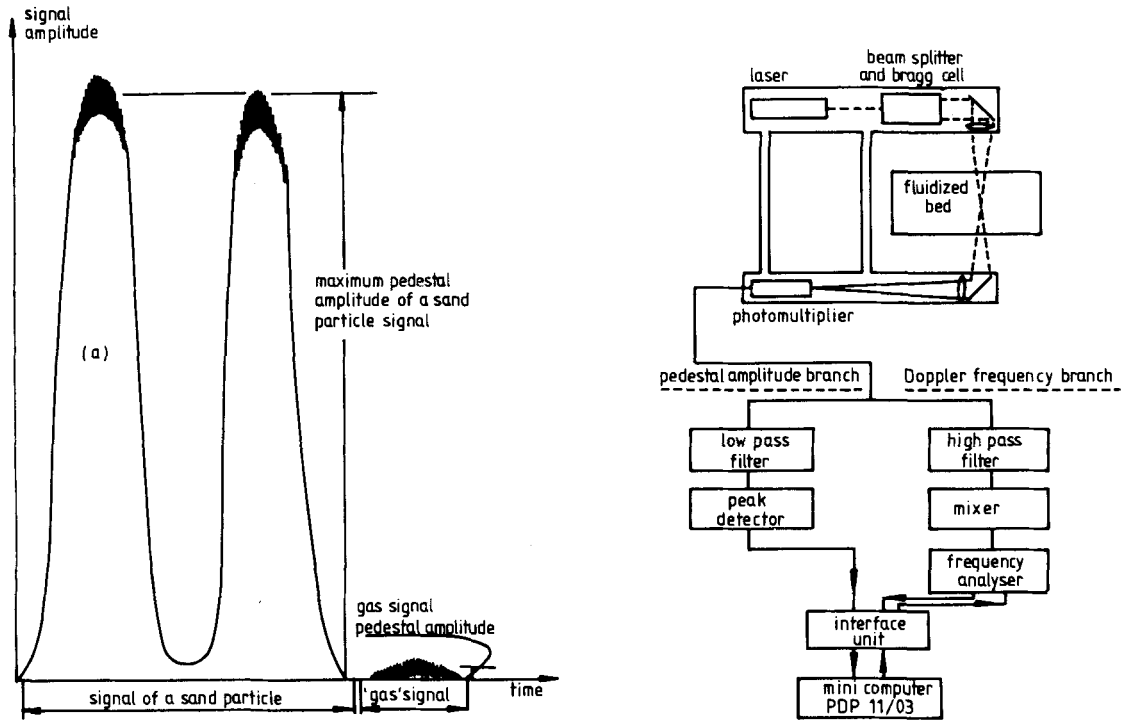

Figure 2. Signal processing.

difference of about two orders of magnitude in the pedestal amplitudes of the signals coming from the different phases. By measuring for each signal the Doppler frequency and the pedestal amplitude, each velocity measurement may be related to its own phase.

The instrumentation is controlled by a PDP 11/03 minicomputer with a dual floppy disk system, running under an assembly language program. A block diagram of the signal processing is shown in panel (b) of Figure 2. The system consists of two branches for simultaneous processing and a computer interface unit. One branch processes the doppler frequency while the other processes the signal pedestal amplitude.

Doppler Frequency Branch. The signal from the photomultiplier is fed through a high pass filter and a mixer (DISA 55 N12) to a frequency counter (Hewlett Packard 5345 A including option 011). A signal of the highest quality having an amplitude above 60 mV peak-to-peak is required. Accordingly, the doppler signal has to be amplified and filtered before processing.

Pedestal Amplitude Detection Branch. The signal from the photomultiplier is fed through a low pass filter to a peak detector unit. The low pass filter removes the doppler frequency oscillation from the photomultiplier signal. The remaining low frequency information is the pedestal amplitude signal. As a particle crosses the control volume, the pedestal amplitude signal changes. The peak detector unit is arranged to detect the maximum pedstal amplitude of every individual particle signal and to convert its value to a digital number.

Once the measurements have been made, the data are read via a Fortran program and scanned to build a histogram of the various pedestal amplitudes. The histogram is displayed on the terminal screen and the operator selects the pedestal amplitude range for the gas and sand signals. A maximum pedestal amplitude value is selected as an upper limit for the gas signal, and a minimum pedestal amplitude value is selected as a lower limit for the sand signal. A ratio of sand signal minimum pedestal amplitude/gas signal maximum pedestal amplitude of about 50 was found to be adequate to secure measurement ranges for the two phases for which the velocities are almost independent of the pedestal amplitude values.

TABLE 1. BED OPERATING CONDITIONS DURING SINGLE-BUBBLE RELEASE EXPERIMENTS

Particle Mean Diameter	0.40 mm
Bed Height (Static)	340 mm
Fluidizing Velocity U_f	0.125 m/s
Bubble Release Cycle Time	1.3 s
Solenoid Valve Opening Time	0.2 s
Pressure at Air Supply Vessel	3.4 bar
Vol. of Air Passed through Valve	1,170 cm^3

Although sand having a rather narrow size distribution formed the bed material some dust and smaller particles are generated by etrition during operation. These particles scatter less light, have a smaller pedestal amplitude and give signals of intermediate strength; the signals from these particles are ignored. Once the range selection for the two phases is determined, mean and rms values are calculated for each phase.

EXPERIMENTAL RESULTS

Single-Bubble Release

Results have been obtained for the single bubble releases superimposed on the bed operated at its minimum fluidizing velocity; a summary of the operating conditions is given in Table 1. The mean and rms velocity data presented have been averaged over 50 consecutive bubble releases. The measurement locations are referred to the coordinate system shown inset on Figure 1.

Figure 3 shows results on the bubble centerline ($x = y = 0$) at various freeboard heights. At $z = 60$ mm the gas velocity initially rises to a maximum (1.5 m/s) which is expectedly greater than that attained by the sand (1.1 m/s). The high gas velocity is probably due to gas escaping from the cloud which envelopes the emerging bubble. There is no information for the next 0.25 s because the rising sand bubble blocks the laser beams. Subsequently we see that the descending sand particles transfer sufficient momentum to the gas to cause the gas velocity to become negative. The gas velocity regains the value U_f somewhat after the sand has settled. This reversing of the gas velocity becomes attenuated with increasing height above the bed until at $z = 260$ mm, where no particles were detected, the gas velocity is essentially zero. Continuity requires that the vertical gas velocity must exceed U_f elsewhere.

The results 100 mm from the bubble axis (Fig. 4) exhibit similar features except that this location is beyond where the sand is being ejected and only negative sand velocities are recorded. Still further from the bubble axis at $x = 200$ mm (Figure 5(a)) we have evidence of gas velocities in excess of U_f at the highest measuring station, $z = 160$. At $z = 60$ mm and for times of less than about 0.3 s, virtually zero vertical gas velocity is recorded. The on-axis results at the same height (Fig. 3) show a significant vertical velocity over this time interval and from continuity considerations we conclude

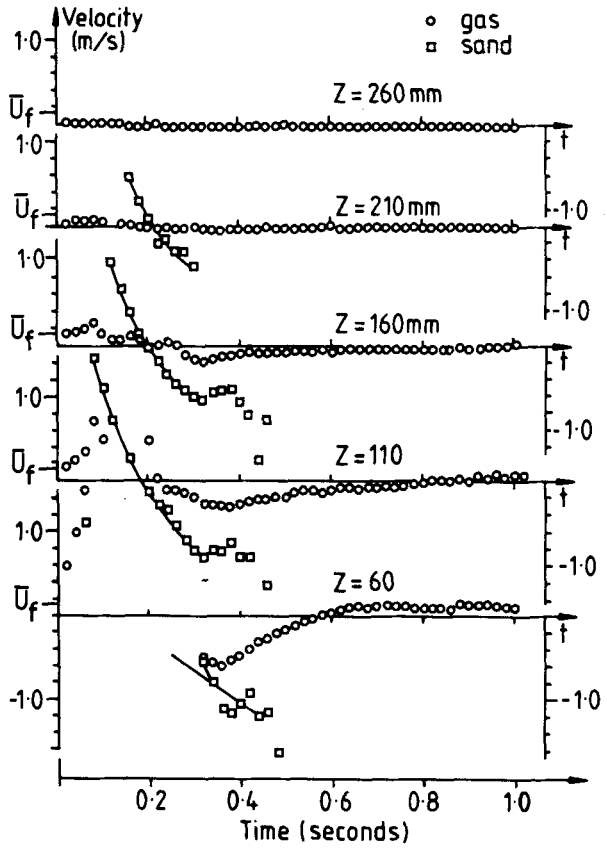

Figure 3. Gas and sand velocity variations with time at locations on the vertical axis: X = 0, Y = 0. Single bubble releases.

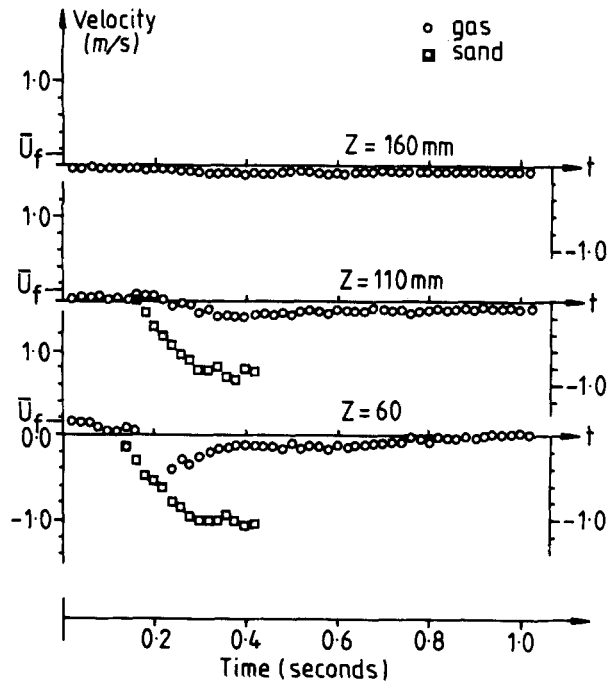

Figure 4. Gas and sand velocity variations with time at locations on the vertical axis: X = 100 mm, Y = 0. Single bubble releases.

that at the $x = 200$ mm location a substantial horizontal and radially inward velocity component exists. We should also note that at a time of about 0.4 s, $x = 0$ and $z = 60$ mm, the gas velocity is downwards whereas at $x = 200$ mm, for the same height and time, it is upwards.

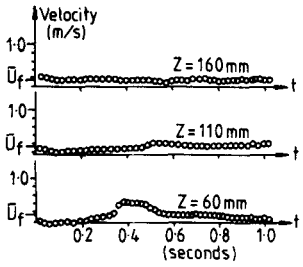

Figure 5(a). Gas and sand velocity variations with time at locations on the vertical axis: X = 200 mm, Y = 0. Single bubble releases.

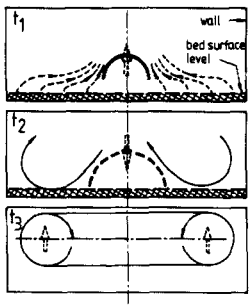

Figure 5(b). Schematic illustration of a toroidal circulation created by a bursting bubble: $t_3 > t_2 > t_1$.

TABLE 2. EXPERIMENTAL OPERATING CONDITIONS

Experiment Designation	dp Particle Mean Diameter (mm)	U_f Fluidizing Velocity	U_{mf} Min., Fluidizing Velocity	Bed Height (Static) (mm)
A1	1.00	0.65	0.5	365
A2	1.00	0.875	0.5	365
HA1	1.00	0.75–1.175	0.5	300
HA2	1.00	1.17	0.5	350
B1	0.40	0.195	0.135	200
B2	0.40	0.235	0.135	200
B3	0.40	0.400	0.135	200
HB1	0.40	0.400	0.135	200
HB2	0.40	0.400	0.135	100–300

The picture of the flow near the bursting bubble which emerges from this evidence is sketched in Figure 5(b). The flow issuing from the bursting bubble entrains surrounding air ($t = t_1$). After the eruption the drag of the descending sand particles on the gas is sufficient to reverse the gas flow ($t = t_2$) and generates a ring vortex ($t = t_3$) which is carried off vertically by the main flow at about the fluidizing velocity ($t > t_3$). We have been able to confirm the existence of this vortex by filming the injection of a smoke tracer; it has important implications for the normally operated bed.

Normal Bed Operation

The conditions of the experiments performed for normal fluidized-bed operation are summarized in Table 2. It can be seen that results have been obtained for two mean sand particle diameters, 0.4 mm and 1 mm, for several fluidizing velocities and bed heights. The principal results of the various experimental trials are now summarized.

Gas-Phase Results. Typical velocity measurements made along the long and short bed axes 500 mm above the bed surface are presented in Figure 6. A remarkable feature is revealed, namely that the mean velocity exhibits a maximum near the walls and a minimum on the bed centerline, the depressed shape being

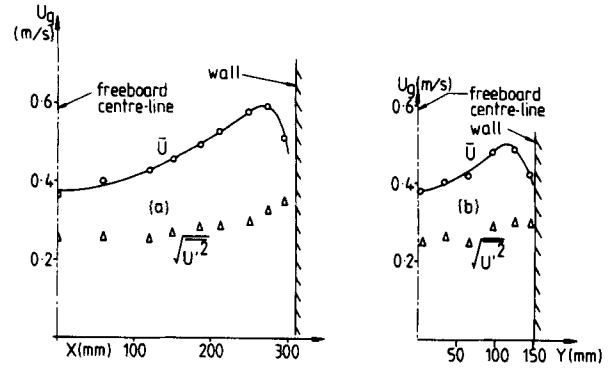

(a) Along x-axis (y = 0). (b) Along y-axis (x = 0).

Figure 6. Variation of gas mean and r.m.s velocities, group HB1 (see Table II) Z = 500 mm. Normal bed operation.

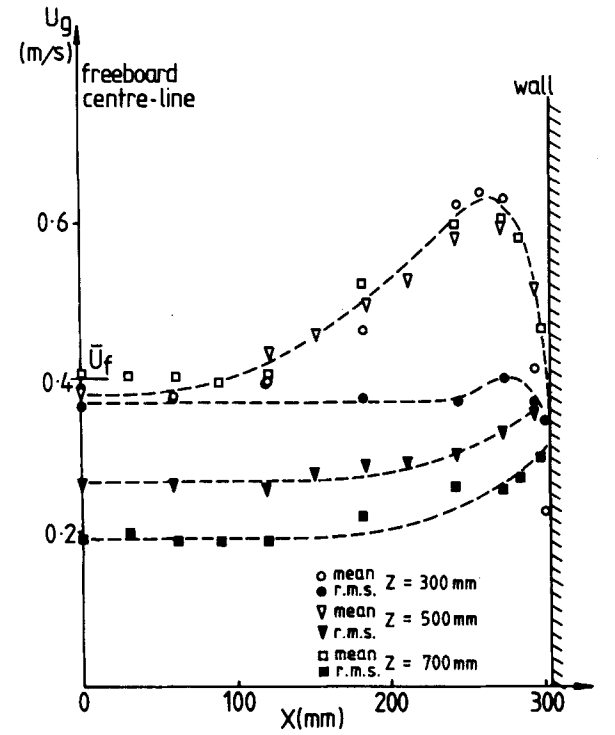

Figure 7. Effect of height above bed. Variation of gas mean and r.m.s. velocities, group HB1 (see Table II), along x-axis, (y = 0), for z = 300, 500 and 700 mm. Normal bed operation.

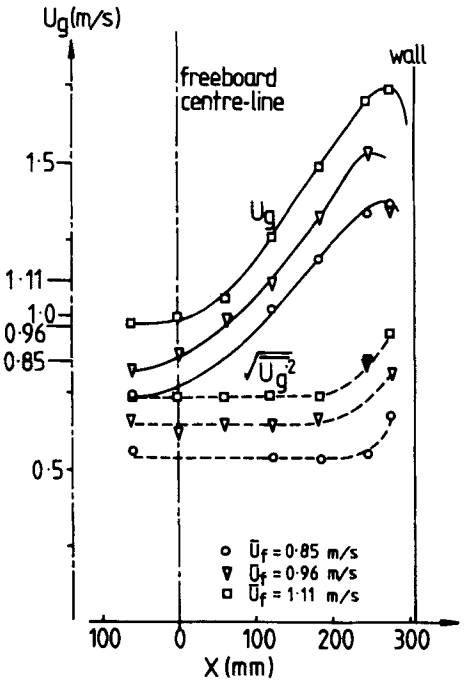

Figure 8. Effect of fluidizing velocity and variation of gas mean and r.m.s. velocities, group HA1 (see Table II), along x-axis (y = 0), for z = 400 mm. Normal bed operation.

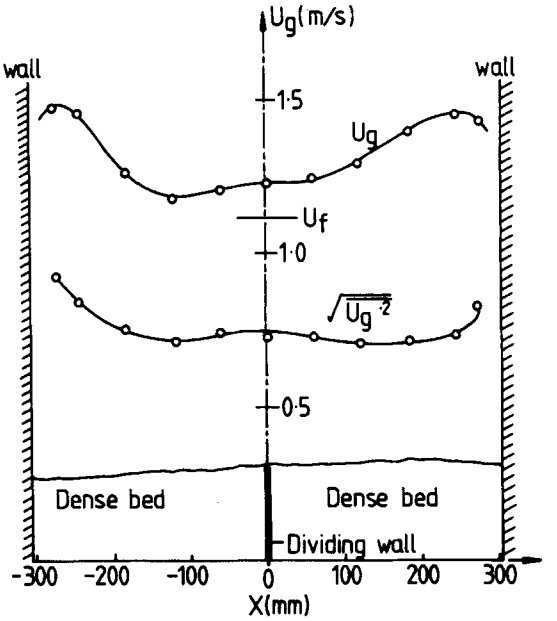

Figure 9. Variation of gas mean and r.m.s. velocities, group HA2 (see Table II), along x-axis (y = 0), z = 400 mm. Normal bed operation.

somewhat more pronounced along the long axis. A three-dimensional portrayal of the velocity profile would resemble a volcanic crater. Profiles along the longer axis at three heights above the dense bed are plotted in Figure 7, the profile of Figure 6 is included. The dipping shape of the mean velocity profile persists at all three heights and, indeed, within the limits of the experimental accuracy it appears not to alter at all. It is also important to observe that the rms velocities, $(\overline{U_g'^2})^{1/2}$, are very large. The centerline values decay with height above the bed as the influence of the bubble bursting becomes progressively smaller, but the near wall values persist.

Further results are presented for the larger 1-mm sand particles in Figure 8 for $z = 400$ mm and for three fluidizing velocities. The depressed profile shape is again revealed, it is apparently unaffected by the fluidizing velocity. The rms velocity increases nearly linearly with $\overline{U}_f$ as would be expected.

In spite of all of this evidence it is difficult to surmise the reason for the peculiar shape of the mean velocity profile. Werther and Moulerus (1973) found that bubbles are more frequently generated near a wall, and part of the explanation for the near wall velocity maximum may be connected with this. In extreme circumstances the near wall flow would tend to a composition of continuous jets. Another part of the explanation may lie in the ring vortex flows which were found to be generated by the single bubble experiments (Figure 5(b)).

The indication in Figure 7 that the near wall rms turbulence persists with height above the dense bed is consistent with the behavior of ring vortices. Also, the fact that the velocity peaks seem not to be smeared by the effects of turbulence diffusion with distance from the dense bed (although admittedly the range of the measurements is not very great) is also evidence of self-preserving vortex motion. At this stage it is tempting to suggest that the ring vortices produces by the random bursts in the central region of the

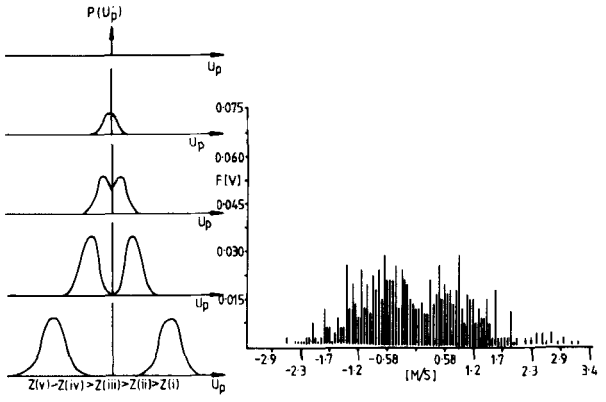

Figure 10. Sand particle probability density functions at different freeboard levels. Normal bed operation.

bed tend to be self-cancelling, but near a wall the bubble bursts are constrained to be more orderly and this combined with their greater frequency results in an additive superposition of the vortices. Confirmation of this explanation requires many more systematic and detailed measurements than we have been able to perform to date, but the simple experiment described in the next paragraph would seem to support it.

We were able to demonstrate convincingly that the velocity maximum is a phenomenon produced by the freeboard wall by introducing a partition in the dense bed only, so splitting the whole bed into two beds of 0.3 m × 0.3 m cross section. The resulting freeboard velocity profile, Figure 9, is not significantly influenced by the presence of the dividing wall. The (small) lack of symmetry evident in this figure was a feature of all of the data and is a result of the difficulty of maintaining the distributor plates in a dirt-free condition.

Sand Phase. In the present tests the particle terminal velocities were essentially all greater than the fluidizing velocities and the freeboard height was so great that there was practically no elutriation. Were it not for the drag forces the mean vertical velocity of the particles would be zero. So the velocity probability density functions at different levels above the dense bed would be expected to have forms sketched in Figure 10(a). The measured distributions do indeed display these forms. However, the positive velocity information is progressively eliminated as the measurement level is decreased, and the actual probability density distribution is correspondingly distorted, because the laser beams are blocked by the densely packed material in the vicinity of an erupting bubble.

Figure 10(b) shows an actual sand velocity histogram (each asterisk represents a computer presented data point) at 400 mm above the bed. At this height the "biasing effect" is nonexistent and the histogram exhibits the expected shape. The sand and gas mean and rms velocities along $y = 0$ for the same height are plotted in Figure 11. The mean sand velocity is nearly zero as required. The sand rms values are large, but this is a reflection of a global variance calculation of the bimodal pdf: a two-part calculation of the properties of the pdf would have been preferable. Visual scrutiny of the relevant sand pdf's suggests that the mean of the absolute velocities is greater near the wall than at the bed axis and this may be due to the increase in gas velocity near the wall. The absolute value of the near wall sand rms also appears larger than the centerline values and this is a reflection of the higher gas rms values there. This general picture is reinforced by the corresponding measurements at the other operating conditions of Table 2.

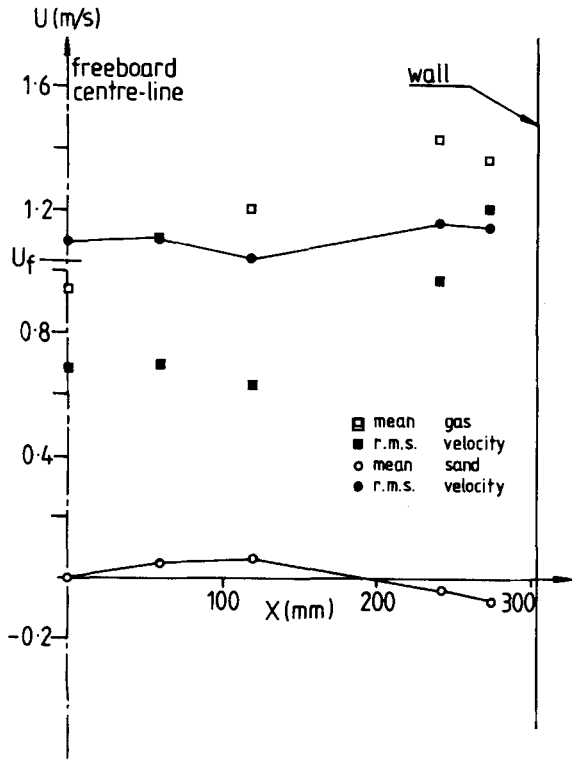

Figure 11. Variation of gas and sand mean and r.m.s. velocities across a horizontal plane group HA1 (see Table II), Y = 0, Z = 400 mm, U_f = 1.03 m/s. Normal bed operation.

ACKNOWLEDGMENT

The authors wish to thank the United Kingdom National Coal Board for their support of this work.

NOTATION

t = time
U = vertical velocity
$\overline{U}$ = time-averaged vertical velocity
U' = fluctuating component of vertical velocity
$\overline{U}_f$ = fluidizing velocity
x = horizontal distance from long axis of freeboard cross section (Figure 1)
y = horizontal distance from short axis of freeboard cross section (Figure 1)
z = vertical distance above static bed surface (Figure 1)

Subscripts

g = gas
p = sand particle

LITERATURE CITED

Andrew, J. M., "Kineticstudy of fluidized solid entrainment," *Ind. and Eng. Chem.*, **52**, No. 1, 85 (1960).

Chen, T. P., and S. C. Saxena, "A theory of solids projection from a fluidized bed surface as a first step in the analysis of entrainment processes," *Fluidization*, 151, Cambridge University Press (1978).

Do, H. T., J. R. Grace, and R. Clift, "Particle ejection and entrainment from fluidized bed," *Powder Tech.*, **6**, 195 (1972).

Durst, F., and B. Elisson, "Properties of laser doppler signal and their exploitation for particle size measurements," Tech. Note SFB 80/TM/82, University of Karlsruhe (1976).

Fournol, A. B., M. A. Bergougnou, and C. G. J. Baker, "Solid entrainment in large gas fluidized bed," *Can. J. of Chem. Eng.*, 51 (1973).

Gosman, A. D., F. C. Lockwood, and A. P. Salooja, "The prediction of cylindrical furnaces gaseous fueled with premixed and diffusion burners," Proceedings of 17th Symp. (Int.) on Combustion, 747, Leeds (1978).

Gugnoni, R. J., and F. A. Zenz, "Particle entrainment from bubbling fluidized beds," *Fluidization*, Proc. of 3rd Found. Conf. on Fluidization, Plenum Publication, England, Eds., Grace and Matser (1980).

Horio, M., A. Taki, Y. S. Hsieh, and I. Muchi, "Elutriation and particle

transport through the freeboard of a gas solid fluidized bed," *Fluidization*, Proc. of 3rd Found. Conf. on Fluidization, Plenum Publication, England, Eds., Grace and Master (1980).
Kunii, D., and O. Levenspiel, "Fluidization engineering," Robert E. Krieger Publishing Co., Huntington, NY (1977).
Leva, M., "Elutriation of fines from fluidized systems," *Chem. Eng. Prog.*, **47**, No. 1, 39 (1951).
Leva, M., and C. Y. Wen, "Elutriation," *Fluidization*, Eds., J. F. Davidson and D. Harrison, Chap. 14, Academic Press, New York (1971).
Levy, Y., "Development of an LDA technique for two phase flows in the freeboard of a fluidized bed," (1982).
Lewis, W. K., E. R. Gilliland, and P. M. Lang, "Entrainment from fluidized beds," *Chem. Eng. Prog. Symp. Ser.*, **58**, No. 38, 65 (1962).
Lin, L., J. T. Sears, and C. Y. Wen, "Elutriation and attrition of char from a large fluidized bed," *Powder Tech.*, **27**, 105 (1980).
Merrick, D., and J. Highley, "Particle size reduction and elutriation in a fluidized bed process," *AIChE Symp. Ser.*, **70**, No. 137, 366 (1972).
Thomas, W. J., P. J. Grey, and S. B. Watkins, "Effect of particle size distribution in fluidization," *British Chem. Eng.*, 176 (1961).
Ungut, A., A. J. Yule, D. S. Taylor, and N. A. Chigier, "Simultaneous velocity and particle size measurements in two-phase flow by laser anemometry," AIAA 16th Aerospace Sciences Meeting, Huntsville, AL (Jan. 16–18, 1978).
Wen, C. Y., and R. F. Hashinger, "Elutriation of solid particles from a dense-phase fluidized bed," AIChE J., **6**, No. 2, 220 (1960).
Werther, J., and O. Moulerus, "The local structure of gas fluidized beds. II: The spatial distribution of bubbles," *Int. J. Multiphase Flow*, **1**, 123 (1973).
Zenz, F. A., and N. A. Weil, "A theoretical-empirical approach to the mechanism of particle entrainment from fluidized bed," *AIChE J.*, **4**, 4 (1958).

Manuscript received June 1, 1982; revision received December 10, and accepted December 14, 1982.

Convective Diffusional Deposition and Collection Efficiency of Aerosol on a Dust-Loaded Fiber

A three-dimensional stochastic model, which is effective for the convective diffusional deposition of aerosol particles, was developed starting from Langevin's equation. The model was utilized to simulate collection and agglomeration processes of particles on a cylindrical fiber. By obtaining the distribution of captured particles on a fiber and the evolution of the collection efficiency of a dust-loaded fiber through the simulation, the effect of Peclet number, interception parameter, and the accumulated mass of particles on them were discussed. Further, the collection efficiency of a dust-loaded fiber was correlated by using a linear function of the accumulated mass of particles in a unit filter volume. Dependence of coefficient in the linear function, collection efficiency raising factor on Peclet number, and interception parameter were also discussed.

CHIKAO KANAOKA and HITOSHI EMI

Department of Chemical Engineering
Kanazawa University
Kanazawa, Japan

and

WIWUT TANTHAPANICHAKOON

Department of Chemical Engineering
Chulalongkorn University
Bangkok, Thailand

SCOPE

Fibrous air filter is composed of various kinds of fine fibers and is capable of collecting fine particles efficiently; the pressure drop across the filter is not so high because of low packing density of the filter. Hence, fibrous air filter is used to purify the air of particles. However, since it is usually operated for a long range of time, it is evident that the fibers in it are more or less covered with collected particles so that the filtering characteristic alters with time. Therefore, it is necessary for the rational design and operation of a filter to know the performance of a dust-loaded filter.

There are few available data and theories on a dust-loaded filter, although enormous number of studies have been done on a clean filter where no particles are captured on the fibers in it. Consequently, fibrous air filter has been designed and operated based on designer's or operator's own experiences or knowhow.

Once aerosol particles are captured on fibers in a filter, they change flow pattern around the fibers, thus affecting the filtering characteristic of the upcoming particles. As a result, they build up particle agglomerates on the fibers with random sizes, shapes and distributions. This was the main reason why the filtering performance of a dust-loaded filter has not been studied for a long time, despite the advance in the filtration theory for a clean filter. However, we know that filter performance does not change so much for a long period of time, if the collection efficiency of the filter is not so good or the aerosol concentration is very low. On the contrary, if the collection efficiency of the filter is high or particle concentration is high, it changes rapidly with operation period. Filter structure and filtration condition also affect the filter performance. These facts suggest that the filter performance is closely related to the dust load in the filter and filtration conditions. Hence, if the collection efficiency of a single fiber with dust load is expressible by some measurable or predictable parameters, the collection efficiency of a filter at arbitrary operation period and conditions can be evaluated.

In this paper, a simple simulation method, using Monte Carlo simulation technique to estimate the growing process of particles dendrites on a fiber by convective Brownian diffusion was proposed. Then, single fiber collection efficiency was evaluated using the simulation results. Finally, it was correlated with the accumulated mass of particles in a filter.